Macromolecules

pubs.acs.org/Macromolecules Article

SCFT-Guided Experimental Fabrication of Double-Diamond Structures in A_1B/A_2B Block Copolymer Binary Blends

Xinyu Wang, Yi Feng, Shuchen Lu, Xueyan Feng,* Guowei Wang,* and Weihua Li*

Cite This: *Macromolecules* 2025, 58, 9776−9785 Read Online

ACCESS | Metrics & More | Article Recommendations | Supporting Information

ABSTRACT: It is well-known that neat AB linear diblock copolymers can form 3-fold double-gyroid (DG) bicontinuous tubular network nanostructures but cannot form thermodynamically stable 4-fold double-diamond (DD) structures. Although theoretical studies have suggested that blending homopolymers or homopolymer-like diblock copolymers into diblock copolymers can stabilize the DD structures in a wide region, experimentally achieving a stable DD structure in diblock copolymer systems still remains challenging. A series of previous studies has demonstrated that the binary blends composed of two A_1B/A_2B diblock copolymers with equal B-blocks but unequal A-blocks exhibit unique capability in stabilizing diverse nonclassical ordered structures by substantially shifting phase boundaries. In this work, we first employed self-consistent field theory (SCFT) to investigate the self-assembly behavior of the A_1B/A_2B blends and identified the parameters for stable DD structures. Our theoretical results reveal that the stability of DD structures is sensitive to the volume fraction of the AB diblock copolymers with shorter A-blocks, as well as sensitive to the length ratio of the two A-blocks. Guided by our theoretical predictions, we synthesized a number of polyisoprene-*b*-polystyrene (PI-*b*-PS) diblock copolymers. We subsequently blended diblock copolymers with varying polyisoprene (PI) lengths and investigated their self-assembled structures across various blending ratios. The DD structure was identified by small-angle X-ray scattering (SAXS) and confirmed by transmission electron microscopy (TEM). Our work demonstrates that experiments guided by reliable SCFT predictions can efficiently discover intriguing nonclassical nanostructures. In addition, our work confirms that this A_1B/A_2B binary blend possesses significant potential for stabilizing diverse novel structures.

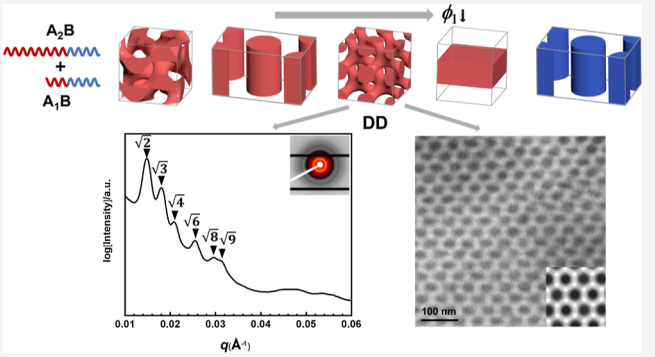

Downloaded via FUDAN UNIV on March 13, 2026 at 02:43:01 (UTC).
See https://pubs.acs.org/sharingguidelines for options on how to legitimately share published articles.

INTRODUCTION

Block copolymers can self-assemble into periodically ordered nanostructures that have promising applications in a wide range of fields.[1−3] Over the past decades, the understanding of the self-assembly behaviors of block copolymers is gradually being improved through the concerted interplay between experiment and theory.[4−6] One of the most applicable class of structures is the bicontinuous tubular network structure due to their unique features of domain connectivity and high interfacial area.[2,7−9] The most common bicontinuous tubular network structure formed by AB-type block copolymers is double-gyroid (DG) that features two interwoven networks with $Ia\bar{3}d$ space symmetry, each comprising a periodic array of three-branched nodes interconnected by struts.[10] In mathematics, there are many other types of bicontinuous tubular network structures, like 4-fold double-diamond (DD) and 6-fold double-primitive (DP).[11,12] In fact, it took a rather long period for experimentalists to finally determine that DG is the stable structure in simple block copolymer melts but not DD.[10,13−19] Though many self-assembled structures can be precisely controlled by tailoring the composition and architecture of block copolymers, how to obtain the DD structure, especially in simple block copolymer systems, remains an interesting and challenging question. Moreover, how to stabilize the DG structure in a wide range of component volume fractions is another issue worth studying because it may broaden the application of DG structure.

It has been known that the higher-valency DD structure has less uniform interfacial curvature or more uneven domain thickness between the strut and the node than the DG structure. When uniform block copolymers self-assemble into the DD structure, they are more frustrated to maintain both uniform curvature and even domain thickness. In other words, the packing frustration of block copolymers in the DD structure is higher than that in the DG structure. This explains why DD is usually less thermodynamically stable than DG in

Received: July 19, 2025
Revised: August 21, 2025
Accepted: August 26, 2025
Published: September 5, 2025

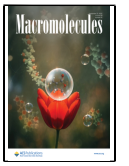

© 2025 American Chemical Society

https://doi.org/10.1021/acs.macromol.5c01972
Macromolecules 2025, 58, 9776−9785

many neat AB-type block copolymers.[20] Accordingly, one straightforward method of stabilizing the DD structure is to add homopolymers into AB diblock copolymers.[21,22] The homopolymer is selectively to fill the central space of each node, alleviating the overstretching caused by the need for the block to extend there. Recent theoretical studies suggest that adding homopolymer-like diblock copolymers into DG-forming diblock copolymers can also effectively stabilize the DD structure, and even the DP structure.[23]

Alternatively, the DD structure may also be stabilized by tailoring the composition and architecture of AB-type block copolymers. Recently, Li et al. have predicted stable DD and DP structures together with the DG structure in neat $A'(A''B)_5$ melts.[24] They have elucidated that the special architecture is able to automatically adjust the conformation of the polymers to adopt to the highly different geometries of the strut and node. More critically, the self-adoptable architecture can control the size difference between strut and node, thus stabilizing the DD and DP structures. In addition, experimentalists have also observed stable high-valency DD or DP structure in some special neat block copolymer melts. Chen et al. observed the DD structure in isotactic polypropylene-*b*-polystyrene (iPP-*b*-PS) and syndiotactic polypropylene-*b*-polystyrene (sPP-*b*-PS) diblock copolymers,[25,26] and Park et al. achieved the DP structure in polystyrene-*b*-poly(ethylene oxide) (PS-*b*-PEO) diblock copolymers with functionalized ends.[27] Nevertheless, understanding the stabilization mechanism of the DD or DP structure still presents a challenge for theory due to the modeling difficulty of these special systems.

Compared to designing the architecture or chemical structures of block copolymers, blending is more economically feasible for experiments.[28−34] For blending, binary blending is clearly a minimal model. More than 20 years ago, Yamaguchi and Hashimoto discovered some interesting self-assembly behaviors in simple AB/AB blends.[35] For example, they observed hexagonal cylinders in the blend composed of two lamella-forming diblock copolymers with largely different molecular weights, which seemed counterintuitive. Ten years later, Li et al. have confirmed the formation of the hexagonal cylinders in this binary blend using self-consistent field theory (SCFT).[36] In recent ten years, a lot of astonishing self-assembly behaviors were predicted by SCFT.[37−39] Our group purposely designed an A_1B/A_2B binary blend composed of two AB diblock copolymers with the same B-blocks but with different A-blocks to significantly broaden the spherical phase region, and thus to stabilize Frank−Kasper structures (σ, A15, and Laves C14 and C15).[40] Moreover, most of these predictions have been confirmed by experiments.[29] In a subsequent work, we predicted another unusual HCP-type "binary" spherical structure in the A_1B/A_2B blend by increasing the length ratio of the two A-blocks.[41]

The main reason for selecting two equal B-blocks in the A_1B/A_2B blend is that two equal B-blocks possess the shortest extension distance, which maximally amplifies the interfacial curvature toward the A-blocks. Accordingly, the phase boundaries can be largely shifted to large volume fraction (f) of A-blocks. In the previous works,[40,41] the volume fraction f_1 of the short A_1-block of one AB diblock copolymer was fixed at a low value so that the neat diblock copolymer forms the classical body-centered cubic (BCC) spherical structure, thus mainly expanding the spherical phase region of the A_1B/A_2B blend. Subsequently, a larger value of f_1 was investigated for enlarging the cylindrical phase region.[42] In a word, f_1 should be a critical parameter in controlling the self-assembly behavior of A_1B/A_2B blends.

In this work, we investigated the self-assembly behavior of A_1B/A_2B binary blends with larger values of f_1, and focused mainly on the formation of bicontinuous tubular network structures, especially the DD structure. We first employed SCFT to construct the phase diagrams of the A_1B/A_2B blend. Under the guide of the calculated phase diagram, we synthesized PI-*b*-PS using living anionic polymerization (LAP) and, prepared the blends to explore their self-assembly structures. It is necessary to mention that Matsushita et al. have found the DD structure in the ternary blends composed of three PS-*b*-PI diblock copolymers with same PS-blocks but different PI-blocks, but they failed to observe the DD structure in the corresponding binary blend.[30] Therefore, our work will answer whether the ternary blend is essential for the stabilization of DD. In addition, our work will clarify that the addition of homopolymers or homopolymer-like diblock copolymers is also not necessary for the formation of DD structure.

METHODS

Self-Consistent Field Theory Simulation. We consider a binary blend of volume V, composed of n_1 A_1B_1 and n_2 A_2B_2 diblock copolymer chains. Each A_iB_i (i = 1 and 2) chain contains $N_{K_i} = f_{K_i}N_i$ statistical K-segments (K = A and B) with $N_{A_i} + N_{B_i} = N_i$. For simplicity, we assume all segments have the same Kuhn length b and density ρ_0. We designate $N_1 = N$ as the reference and set $N_2 = \gamma N$. The blending system can be described either in the canonical ensemble[43] or in the grand canonical ensemble.[44] In the canonical ensemble, the concentration of A_1B_1, $\phi_1 = n_1N_1/(n_1N_1 + n_2N_2)$, is specified. Whereas, in the grand canonical ensemble, the concentration is variable and regulated by the chemical potential, μ_i (i = 1 and 2). Only one of the two chemical potentials, μ_1 and μ_2, is independent due to the incompressibility condition, and we set $\mu_1 = 0$ for convenience. Accordingly, ϕ_1 is regulated by μ_2 or, equivalently, the activity $z = z_2 = \exp(\mu_2/k_BT)$, where k_BT is the unit of thermal energy at temperature T and k_B is the Boltzmann constant. For a given set of chemical potentials, two different ordered phases with equal grand-canonical free energies usually possess different concentrations, leading to the coexistence region of the two phases with respect to the concentration. Under the approximations of the mean-field treatment and Gaussian-chain model, the free energy of the binary A_1B_1/A_2B_2 blend in the canonical ensemble at temperature T is expressed as[43]

$$\frac{NF}{V\rho_0 k_BT} = -\phi_1 \ln Q_1 - \frac{(1-\phi_1)}{\gamma}\ln Q_2 + \frac{1}{V}\int d\mathbf{r}\{\chi N\phi_A(\mathbf{r})\phi_B(\mathbf{r}) - w_A(\mathbf{r})\phi_A(\mathbf{r}) - w_B(\mathbf{r})\phi_B(\mathbf{r}) - \eta(\mathbf{r})[1-\phi_A(\mathbf{r})-\phi_B(\mathbf{r})]\} \quad (1)$$

where $\phi_K(\mathbf{r})$ (K = A and B) is the spatial distribution of the volume fraction of K-block and $w_K(\mathbf{r})$ is its conjugate potential field. $\eta(\mathbf{r})$ is a Lagrange multiplier used to enforce the incompressibility condition, $\phi_A(\mathbf{r}) + \phi_B(\mathbf{r}) = 1$. The two quantities Q_1 and Q_2 are the single chain partition functions of the two types of diblock copolymers interacting with the mean fields of $w_A(\mathbf{r})$ and $w_B(\mathbf{r})$ produced by surrounding chains, which can be written as

$$Q_1 = \frac{1}{V}\int d\mathbf{r} q_1(\mathbf{r}, s)q_1^\dagger(\mathbf{r}, s) \quad (2)$$

$$Q_2 = \frac{1}{V}\int d\mathbf{r} q_2(\mathbf{r}, s)q_2^\dagger(\mathbf{r}, s) \quad (3)$$

where $q_i(\mathbf{r}, s)$ and $q_i^\dagger(\mathbf{r}, s)$ (i = 1 and 2) are the propagator functions giving the probability of finding the s-segment on the chain contour at

https://doi.org/10.1021/acs.macromol.5c01972
Macromolecules 2025, 58, 9776−9785

spatial position **r** starting from the free ends of A-block and B-block, respectively. These propagator functions satisfy the modified diffusion equations that can be found in the literature.[41,45,46]

In our SCFT calculations, $R_g = (N/6)^{1/2}b$ is chosen as the unit of spatial length, and the contour variable $s \in [0, 1]$ for A_1B_1, while $s \in [0, \gamma]$ for A_2B_2. By minimizing the free energy with respect to both the volume fraction $\phi_K(\mathbf{r})$ and the potential field $w_K(\mathbf{r})$ (where K = A, B), we obtain the standard SCFT equations, which are also well-documented in the literature.[41,45,46]

To determine the phase coexistence regions, we construct the phase diagram through SCFT calculations in the grand canonical ensemble, where the free energy (grand potential) is expressed in units of k_BT as[47]

$$\frac{NF}{V\rho_0 k_B T} = -Q_1 - zQ_2 + \frac{1}{V} \int d\mathbf{r}\{\chi N\phi_A(\mathbf{r})\phi_B(\mathbf{r}) - w_A(\mathbf{r})\phi_A(\mathbf{r}) - w_B(\mathbf{r})\phi_B(\mathbf{r}) - \eta(\mathbf{r})[1 - \phi_A(\mathbf{r}) - \phi_B(\mathbf{r})]\} \quad (4)$$

where $z = z_2 = \exp(\mu_2/k_BT)$ is the activity. In the grand canonical ensemble, the volume fraction distributions take a different form from those in the canonical ensemble, though all other SCFT equations are the same. More details about these equations can be found in literature.[41,45,46]

In the grand canonical ensemble, the spatial average concentration ϕ_1 is conjugated to z, and thus determined by

$$\phi_1 = Q_1 = 1.0 - z\gamma Q_2 \quad (5)$$

Both the canonical and grand canonical ensemble formulations of SCFT can be numerically solved through standard iterative approaches. We utilize the pseudospectral method[48,49] to solve the modified diffusion equations, combined with Anderson mixing[50] to accelerate convergence to equilibrium SCFT solutions. Previous studies have demonstrated that the pseudospectral method achieves reliable free energy accuracy when using enough fine grids and small contour steps. A grid spacing of smaller than $0.2R_g$ and a chain contour step size of $\Delta s \leq 0.01$ are used in our calculations.

Experimental Methods. Polyisoprene-*b*-polystyrene (PI-*b*-PS) diblock copolymers with various volume fractions were synthesized by living anionic polymerizations in cyclohexane at room temperature under a purified nitrogen atmosphere using *n*-butyllithium as the initiator. The polymerization of isoprene was conducted for 4 h, followed by a 2 h styrene polymerization. Detailed procedures can be found in the previous work.[51] The number-average molecular weight (M_n) and molecular weight distribution (M_w/M_n) of the copolymers were measured using size exclusion chromatography (SEC) (Figure S1). The volume fractions were determined by SEC and proton nuclear magnetic resonance (^{1}H NMR) spectra (Figure S2). The molecular characteristics of samples are summarized in Table 1.

Under the guide of the SCFT, we synthesized a series of PI-*b*-PS diblock copolymers with nearly identical PS-blocks (approximately 30,000 g/mol) and varying PI blocks with molecular weight ranging from 13,700 to 76,300 g/mol. The IS33 and IS35 samples were selected for binary blending with other five samples with relatively longer PI-blocks. The volume fractions of the samples IS33 and IS35 in the series of binary blends varied from 10/90 to 90/10 in 10% steps. All samples were prepared via solution casting from 5 wt % THF solutions, followed by slow solvent evaporation at room temperature (RT). To ensure complete THF removal, the cast films were first dried under vacuum for 24 h. Subsequently, the samples were thermally annealed at 150 °C under high vacuum for over 24 h, followed by rapid quenching in liquid nitrogen.

The microphase separation morphologies were characterized using transmission electron microscopy (TEM) and small-angle X-ray scattering (SAXS) techniques. For TEM analysis, ultrathin sections (90 nm thickness) were prepared using a Leica Ultracut Microtome (FC7-UC7 Leica Ltd.) at −90 °C, followed by I_2 vapor staining for 12 h at room temperature to enhance contrast. The PI microdomains were stained and looked dark because of selective staining with I_2 vapor. TEM imaging was performed at room temperature using a field-emission TEM (Talos F200S G2 Thermo Fisher Ltd.) operated at 200 kV. SAXS measurements were performed using both laboratory and synchrotron radiation sources. Laboratory-scale SAXS data were collected on a Xenocs Xeuss 2.0 instrument with an X-ray wavelength of $\lambda = 1.54$ Å, using a detector distance of ∼2.3 m and 300 s exposure time. Synchrotron SAXS was conducted at the Shanghai Synchrotron Radiation Facility (SSRF) with a wavelength of $\lambda = 1.24$ Å and detector distance of ∼2.2 m. The magnitude of the scattering vector (q) is given by $q = 4\pi/\lambda \sin(\theta/2)$, where λ is the wavelength of the X-ray and θ is the scattering angle.

Table 1. Molecular Characteristics of PI-*b*-PS Diblock Copolymers

sample[a]	f_{PI}[b]	$M_{n,PI}$[c]	$M_{n,PS}$[b,c]	M_w/M_n[c]	N[d]	γ_{IS35}[e]	γ_{IS33}[f]
IS33	0.33	13,700	31,800	1.09	694		1
IS35	0.35	14,500	31,700	1.09	708	1	
IS43	0.43	19,500	30,300	1.09	771	1.09	1.11
IS52	0.52	25,600	27,800	1.10	838	1.18	1.21
IS64	0.64	39,800	26,600	1.10	1061	1.50	1.53
IS71	0.71	62,200	29,400	1.09	1480	2.09	2.13
IS74	0.74	76,300	31,000	1.06	1742	2.46	2.51

[a]Each sample is labeled as IS*xx*, where *xx* corresponds to the volume fraction of PI in the sample. [b]The calculation is performed using ^{1}H NMR, with the known densities of polyisoprene (ρ_{PI} = 0.830 g/cm^3) and polystyrene (ρ_{PS} = 0.969 g/cm^3). [c]Determined by SEC. [d]The number-average degree of polymerization N was derived from the equation $N = (M_{n,PS}\rho_{PS}^{-1} + M_{n,PI}\rho_{PI}^{-1})N_{av}^{-1}v^{-1}$, where N_{av} is the Avogadro number and v = 118 Å^3 is the segment volume. [e]$\gamma_{IS35} = N_x/N_{IS35}$, where N_x is the number-average degree of polymerization of all blended samples. [f]$\gamma_{IS33} = N_x/N_{IS33}$.

RESULTS AND DISCUSSION

SCFT Results. The self-assembly behavior of the A_1B/A_2B blends with equal B-blocks is mainly controlled by three parameters, the volume fraction of A_1-block (f_1), the length ratio of the two copolymers (γ) and the concentration of A_1B (ϕ_1). In previous works, a relatively small value of f_1 like f_1 = 0.15 or f_1 = 0.23 was chosen to explore the self-assembly behavior for the formation of spherical structures. Here we first consider a rather larger value of f_1 = 0.36 and χN = 20, of which the pure diblock copolymer forms the DG structure (Figure S3), to construct the two-dimensional phase diagram at the $\gamma-\phi_1$ plane, focusing on the network structures. Accordingly, we selected candidate structures from those structures that are usually neighboring to or often compete with DG, including hexagonal array of cylinders (C_6), lamellae (L), DD and *Fddd* (O^{70}) (Figure S4).

The phase diagram of the A_1B/A_2B blend with respect to γ and ϕ_1 is constructed by SCFT calculations in the grand canonical ensemble as shown Figure 1. When $\gamma < 2.9$, corresponding to the volume fraction of A_2B diblock copolymer $f_2 < 0.779$, the DG structure transfers to L as the long A_2B diblock copolymer is added. Due to the increasing difference in length between the two A-blocks with increasing γ, the coexistence region between DG and L progressively widens. Interestingly, the DD and C_6 structures appear before the transition from DG to L for $\gamma > 2.9$, leading to the transition from DG to DD, C_6 and then back to DG. Both DD and C_6 structures exhibit considerable stability windows. Specifically, the phase region of DD spans the range of $2.9 < \gamma < 3.8$, and the largest width is $\Delta\phi_1 \approx 0.06$ that is enough for experiments to target the DD structure. The relevant transition

https://doi.org/10.1021/acs.macromol.5c01972
Macromolecules 2025, 58, 9776−9785

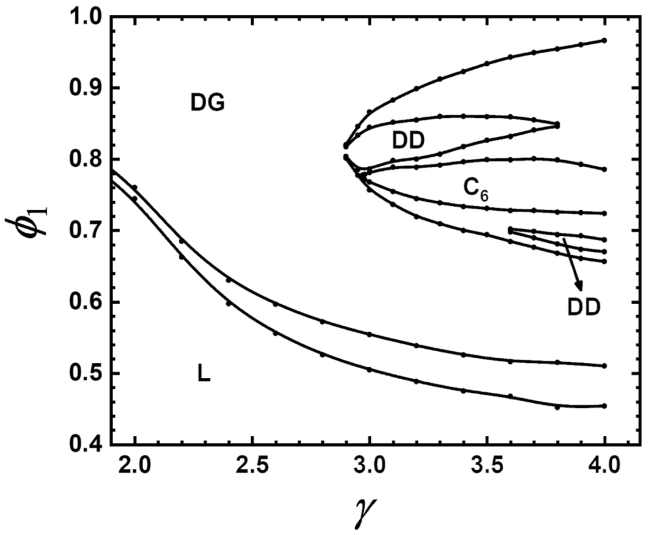

Figure 1. Phase diagram with respect to γ and ϕ_1 for the A_1B/A_2B binary blend with χN = 20 and f_1 = 0.36, where unmarked regions indicate the coexistence regions between each pair of adjacent phases.

mechanism will be discussed later. Note that there exists another narrow DD phase region below the C_6 region for γ > 3.6, which may potentially correspond to other unconsidered structures. Since our primary focus lies in theoretically guiding the experimental realization of the DD structure, here we will not elaborate further on this particular aspect.

It has been known that the phase behavior of the A_1B/A_2B blend is sensitively dependent on f_1 of A_1B diblock copolymer. We consider another value of f_1 = 0.33, corresponding to the C_6 structure of the pure diblock copolymer (Figure S3), to see whether the DD structure can be formed in the blend. The phase diagram in Figure 2 indicates that the C_6 structure transfers to DG and then to L. Within the considered range of 2.0 < γ < 3.8, no DD structure is observed. This implies that a larger value of f_1 would be necessary to achieve a stable DD structure.

Although our SCFT results cannot provide quantitative guidance to experiments, they do offer qualitative insights. The

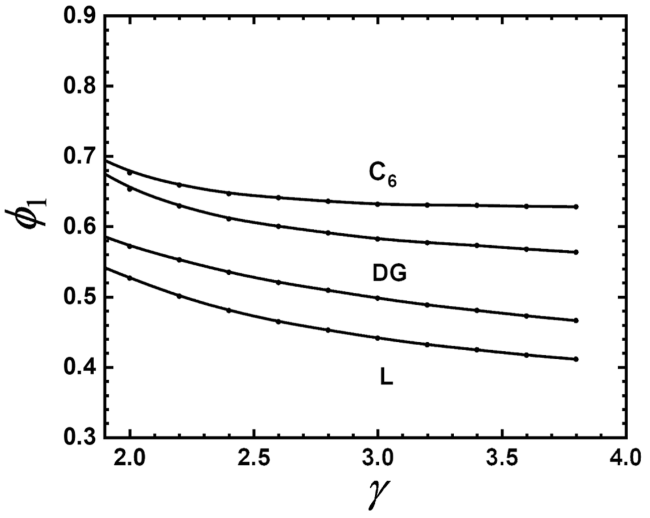

Figure 2. Phase diagram with respect to γ and ϕ_1 for the A_1B/A_2B binary blend with χN = 20 and f_1 = 0.33, where unmarked regions indicate the coexistence regions between each pair of adjacent phases.

theoretical results reveal that one of the most critical factors for forming the DD structure is to select f_1 preferably within the DG phase region of the pure diblock copolymer. The second important factor is to maintain equal B-block lengths while ensuring sufficient difference in the molecular weights between the two copolymers (or between the two A-blocks). Another nontrivial factor is that the DD structure typically emerges in the region of relatively large ϕ_1. Based on these guidelines, we synthesized two short diblock copolymers (IS33 with f_1 = 0.33 and IS35 with f_1 = 0.35) and five long diblock copolymers (IS43 with f_2 = 0.43, IS52 with f_2 = 0.52, IS64 with f_2 = 0.64, IS71 with f_2 = 0.71 and IS74 with f_2 = 0.74). Subsequently, we investigated the self-assembly behavior of the blend systems by pairwise mixing the copolymers with short and long PI blocks.

Experimental Verification. We first examine the self-assembled morphologies of the pure IS35 and IS33 samples (Figure 3). For IS35, the relative scattering peak ratios are $\sqrt{6}$, $\sqrt{8}$, $\sqrt{14}$ and $\sqrt{22}$, corresponding to the DG structure. And the scattering peak ratios for IS33 are 1, $\sqrt{3}$, 2, $\sqrt{7}$ and 3, evidencing the C_6 structure. Therefore, the two samples we synthesized qualitatively match the short diblock copolymers considered in our SCFT calculations.

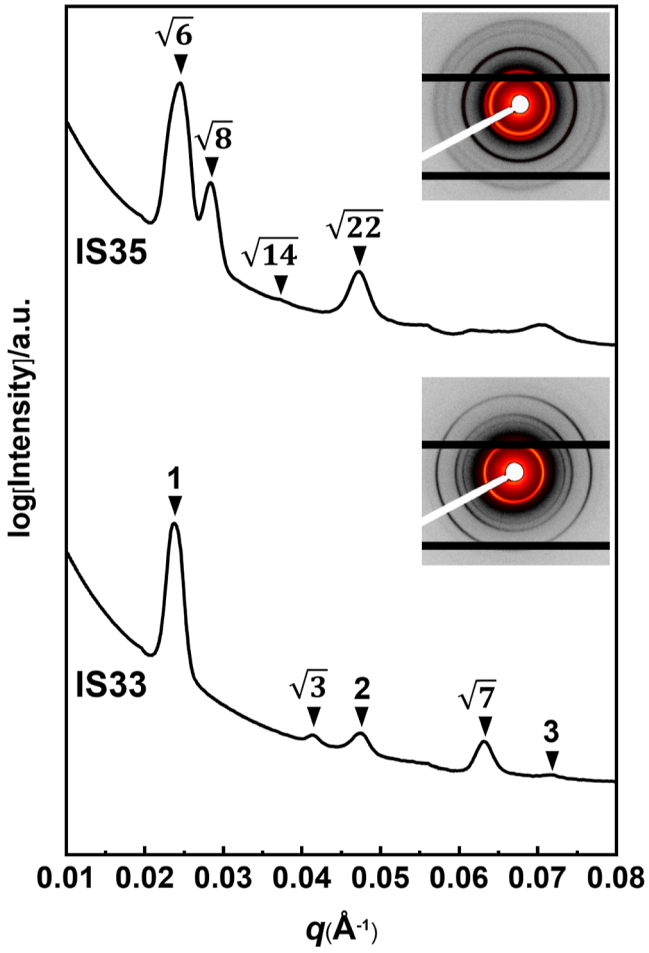

Figure 3. Synchrotron SAXS profiles of IS35 and IS33. The sequence of peaks in SAXS profiles is marked by inverted triangles. The original 2D SAXS data are presented as insets.

We first blended IS71 and IS74 with IS35, respectively, corresponding to γ = 2.09 and γ = 2.46. For the IS35/IS71

https://doi.org/10.1021/acs.macromol.5c01972
Macromolecules 2025, 58, 9776−9785

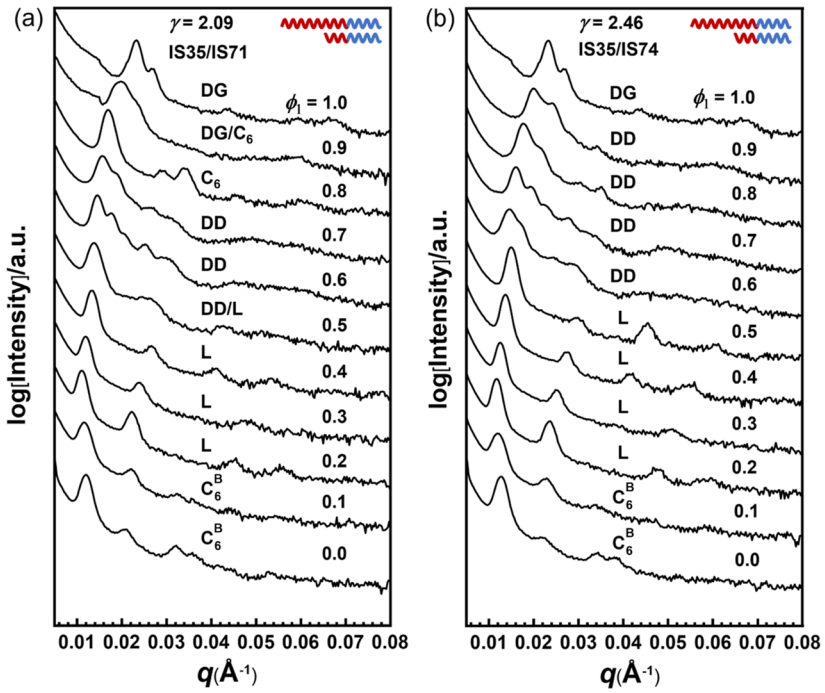

Figure 4. SAXS profiles of blends (a) IS35/IS71 and (b) IS35/IS74 at different ϕ_1 values, where ϕ_1 represents the volume fraction of IS35 in the IS35/IS71 and the volume fraction of IS33 in the IS33/IS71. The schematic in the upper right corner of each panel illustrates the two copolymer chains.

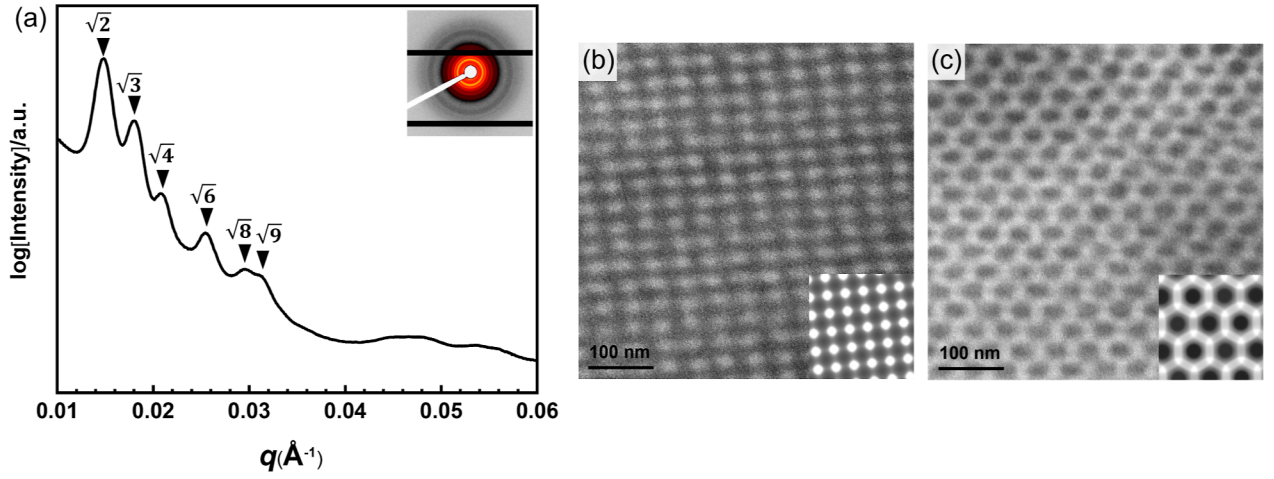

Figure 5. Synchrotron SAXS profiles of IS35/IS71 blends with $\phi_1 = 0.6$ (a). The SAXS peak sequence is denoted by inverted triangles and the inset displays the original two-dimensional scattering data. Panels (b,c) present TEM images of the sample IS35/IS71 with $\phi_1 = 0.6$. The insets in the TEM images show the simulated (100) and (111) planes of the DD structure.

blends (Figure 4a), the SAXS profiles suggest that the self-assembled structures change from DG to C_6 at $\phi_1 = 0.8$, DD at $\phi_1 = 0.7$ and $\phi_1 = 0.6$, L at $0.2 \leq \phi_1 \leq 0.4$, and finally to hexagonal array of PS-cylinders (C_6^B, same as the bulk phase of the pure IS71 sample) as the concentration of IS71 increases or ϕ_1 decreases. For the IS35/IS74 blends (Figure 4b), the DD structure is observed in a wider range of $0.6 \leq \phi_1 \leq 0.9$, and the C_6 structure does not appear in the transition sequence. These experimental results are in qualitative agreement with our SCFT predictions.

To confirm the formation of the DD structure, we performed synchrotron SAXS measurements to obtain higher-resolution scattering peaks for the morphology formed by the IS35/IS71 blend with $\phi_1 = 0.6$, along with corresponding TEM images. The SAXS profile (Figure 5a) clearly contains scattering peak series with q ratios of $\sqrt{2}$, $\sqrt{3}$, $\sqrt{4}$, $\sqrt{6}$, $\sqrt{8}$ and $\sqrt{9}$, which are the typical scattering peaks of DD. Moreover, the TEM images in Figure 5b,c match the simulated (100) and (111) planes of the DD structure well.

Figure 6 summarizes the self-assembled structures of the binary blends composed of one of the two short diblock copolymers (IS35 and IS33) and one of the five long diblock copolymers. The corresponding γ-values for the five long chains relative to the IS35 chain are 1.09, 1.18, 1.50, 2.09, and 2.46, respectively, while they become 1.11, 1.21, 1.53, 2.13, and 2.51 for IS33. As mentioned before, the DD structure is observed at $\gamma = 2.09$ and 2.46 for the IS35-containing blends. For $\gamma \leq 1.5$, the DG structure directly transfers to L with

https://doi.org/10.1021/acs.macromol.5c01972
Macromolecules 2025, 58, 9776−9785

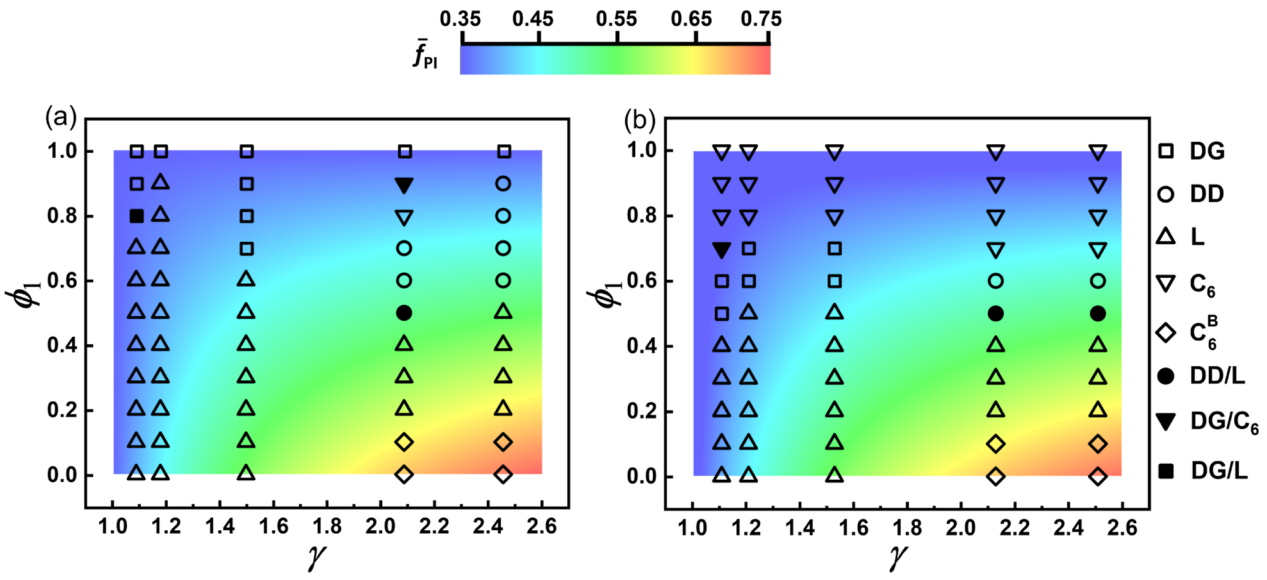

Figure 6. Experimental phase diagrams of the binary blends of IS35/IS43 (γ = 1.09), IS35/IS52 (γ = 1.18), IS35/IS64 (γ = 1.50), IS35/IS71 (γ = 2.09) and IS35/IS74 (γ = 2.46) (a) and IS33/IS43 (γ = 1.11), IS33/IS52 (γ = 1.21), IS33/IS64 (γ = 1.53), IS33/IS71 (γ = 2.13) and IS33/IS74 (γ = 2.51) (b). The color spectrum represents the average volume fraction of PI-blocks in the blends.

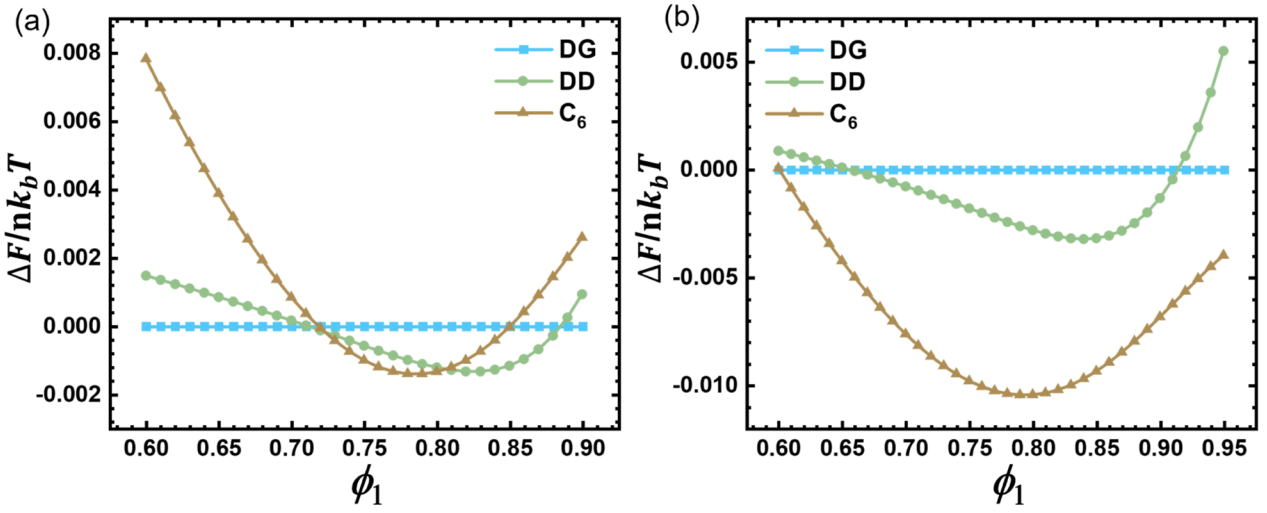

Figure 7. Free-energy comparison among the DG, DD, and C_6 structures along varying ϕ_1 at fixed γ = 3.4 for f_1 = 0.36 (a) and f_1 = 0.33 (b).

decreasing ϕ_1, without the appearance of DD (Figure 6a). Although the DD structure is also observed in the IS33-containing blends with γ = 2.13 and 2.51 (Figure 6b), its region is noticeably narrower than that in Figure 6a. Moreover, the transition sequence at $\gamma \leq 1.53$ in Figure 6b becomes $C_6 \rightarrow$ DG $\rightarrow$ L, which is due to the generally smaller average volume fraction of A-blocks and thus higher curvature of the IS33-containing blends than the counterparts of IS35. In this paper, curvature refers to the average mean curvature. This comparison indicates that f_1 of short diblock copolymer is more conducive to stabilizing the DD structure within their DG phase region than in the C_6 region, which qualitatively aligns with our theoretical conclusion.

There exist some discrepancies between the transition sequence of DG $\rightarrow$ C_6 $\rightarrow$ DD $\rightarrow$ L experimentally observed in the IS35/IS71 blends and that of DG $\rightarrow$ DD $\rightarrow$ C_6 $\rightarrow$ DG $\rightarrow$ L predicted by SCFT accompanied by a decrease in ϕ_1 in Figure 1, mainly manifested by the appearance of the C_6 structure at the side of smaller or larger ϕ_1. In fact, both phase sequences exhibit a common characteristic: the curvature first increases and then decreases (the curvature of the C_6, DG and DD structures in SCFT see Figure S5). This is primarily because the curvature effect is governed by two factors, the average volume fraction of A-blocks ($\bar{f}_A$) and the local segregation of the two distinct A-blocks.[35,36,40,41] Specifically, the spontaneous curvature bending toward A-blocks commonly decreases with increasing $\bar{f}_A$. On the other hand, previous works have verified that the curvature can be amplified by the core−shell distribution of long and short A-blocks inside the curvature in the A_1B/A_2B blend with equal B-blocks. For different f_1, the maximal curvature may appear at the different values of ϕ_1, where the C_6 structure is preferably formed.

The color spectrum for the magnitude of $\bar{f}_{PI}$ in Figure 6 shows that DG is formed in the IS35-containing blends with $0.35 \lesssim \bar{f}_{PI} \lesssim 0.437$ that is considerably wider than that of pure PI-*b*-PS diblock copolymer. In comparison, the DD structure is

https://doi.org/10.1021/acs.macromol.5c01972
Macromolecules 2025, 58, 9776−9785

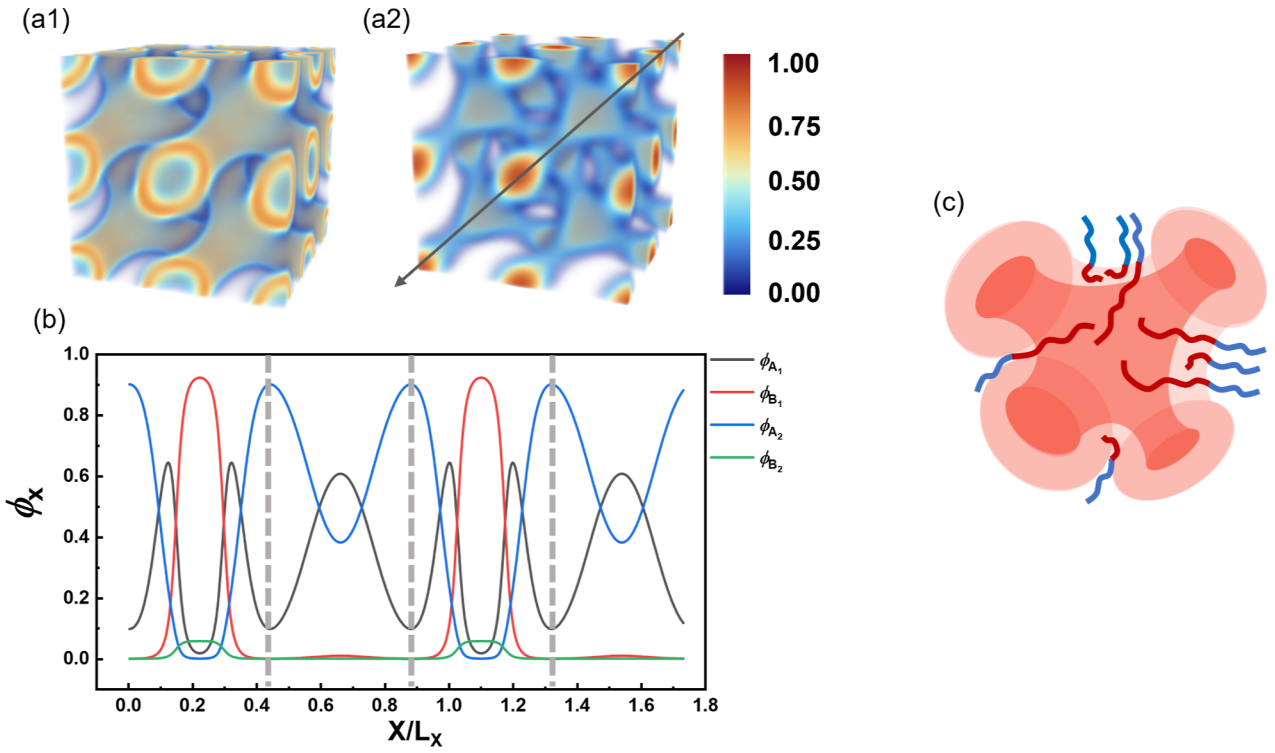

Figure 8. 3D density distributions of (a1) short and (a2) long A-blocks in the stabilized DD structure under conditions of $\gamma = 3.4$ and $\phi_1 = 0.84$. (b) Displays the volume fraction distributions of different blocks along the body diagonal indicated by the arrow in (a2), with the gray dashed lines representing the nodes in the DD structure. (c) Schematics illustrating the chain packing of two different AB diblock copolymers in the DD structure.

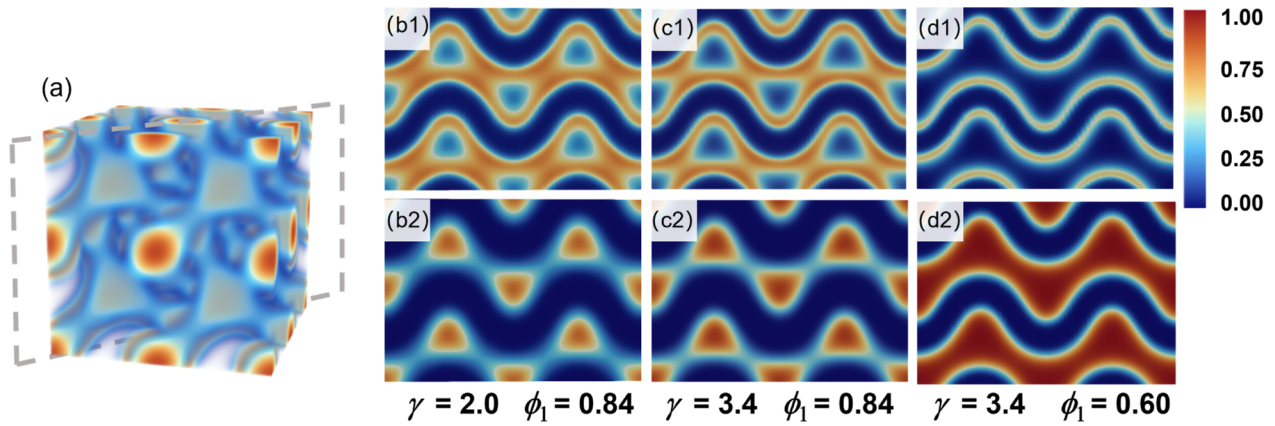

Figure 9. Two-dimensional density distributions of A_1- and A_2-blocks in the cross-section of the DD structure along the (110) plane (dashed-box direction in (a)) for $\gamma = 2.0$, $\phi = 0.84$ (b1,b2), for $\gamma = 3.4$, $\phi = 0.84$ (c1,c2), and for $\gamma = 3.4$, $\phi = 0.60$ (d1,d2).

observed in an even wider range of larger $\overline{f}_{PI}$, that is, $0.389 \lesssim \overline{f}_{PI} \lesssim 0.506$. In the phase diagram of the IS33-containing blends, the phase region of DD is significantly narrowed. This is because f_1 of the short diblock copolymer is located in the C_6 region of rather high curvature, the binary blend formed after adding the long diblock copolymer maintains the C_6 structure over a broad range of ϕ_1 where the curvature first increases and then decreases, thereby compressing the DD region.

Mechanism Explanation. The free-energy comparisons in Figure 7 show that the addition of the long A_2B diblock copolymer can stabilize the DD structure over the DG structure in a considerable region of ϕ_1 for both $f_1 = 0.33$ and $f_1 = 0.36$ (typical free-energy comparisons containing more phases are shown in Figure S6). Note that DD is always less stable than DG in the pure AB diblock copolymer with $f_1 = 0.33$ or $f_1 = 0.36$ (i.e., at $\phi_1 = 1$). These results clarify that the second diblock copolymer serves as the critical factor of stabilizing the DD structure over the DG structure, which will be discussed later. The range of $0.66 \lesssim \phi_1 \lesssim 0.91$ where DD is more stable than DG at $f_1 = 0.33$ is wider than $0.71 \lesssim \phi_1 \lesssim 0.88$ at $f_1 = 0.36$, however, the DD structure remains less stable than the C_6 structure within this entire range of $0.60 < \phi_1 < 0.95$ at $f_1 = 0.33$. Although the range of ϕ_1 where DD is more stable than DG significantly narrows as f_1 increases from 0.33 to 0.36, there still exists a region within this ϕ_1 range where DD is also more stable than C_6, which corresponds to the thermodynamic stability region of the DD structure. Therefore,

https://doi.org/10.1021/acs.macromol.5c01972
Macromolecules 2025, 58, 9776−9785

to achieve a stable DD structure, we must not only enhance the stability of DD relative to DG, but also need to prevent the C_6 structure from occupying the stability region of DD due to the increased curvature by the core−shell effect in the binary blends. This is why we need to choose a rather high value of f_1.

The addition of the long diblock copolymer ($N_{A_2} \gg N_{A_1}$) not only increases $\overline{f}_A$ but also amplifies the curvature effect, shifting the phase boundaries toward large $\overline{f}_A$ and thus favoring the formation of DD. Another critical factor is that the long A_2-block can preferentially extend to fill the central space of the bulkier node of DD, relieving the high packing frustration. Figure 8(a1,a2) respectively display the three-dimensional density distributions of the short A_1-blocks and the long A_2-blocks in the DD structure at $\gamma = 3.4$ and $\phi_1 = 0.84$. The short A_1-blocks are primarily distributed on the surface of the DD structure, while the long A_2-blocks are mainly located in the interior of the DD structure, especially preferentially extending to the center of the bulkier node. From the one-dimensional density distributions (Figure 8b), it can be observed that this localized segregation effect is more pronounced at the nodes of the DD structure.

Moreover, the highly distinct curvatures of the two diblock copolymers facilitate their local segregation, enabling adaptation to the largely variable interfacial curvature of the DD structure. We obtain stable DD structure regions at both large γ and ϕ_1, which is related to the local segregation of the A-blocks. When γ is small (Figure 9(b1,b2), $\gamma = 2.0$), the length difference between A_1-blocks and A_2-blocks is relatively minor, resulting in insignificant local segregation between A_1-blocks and A_2-blocks. The excessive stretching of the shorter A_1-blocks becomes entropically unfavorable for the system, thereby making the DD structure unstable. When ϕ_1 is small (Figure 9(d1,d2), $\phi_1 = 0.6$), the large volume fraction of A_2-blocks in the phase domain leads to the overconcentrated packing of the long A_2-blocks in the nodes and struts of the DD structure, which is also unfavorable from the aspect of spontaneous curvature. Therefore, stable DD structures only form under appropriate γ and ϕ_1 conditions (Figure 9(c1,c2)), where the localized segregation effect can effectively alleviate the packing frustration of the blocks.

CONCLUSION

In summary, we have investigated the self-assembly behavior of A_1B/A_2B binary blends combining self-consistent field theory (SCFT) calculations and experiments, focusing on the exploration of thermodynamically stable DD structure. The A_1B/A_2B blend is purposely designed to be composed of two AB diblock copolymers with equal B-blocks but unequal A-blocks, aiming to largely amplify the effect of spontaneous curvature toward A-blocks. We first employ SCFT to identify the stable region of the DD structure in the binary blend system. The analysis focuses on two key parameters: the length ratio γ and the volume fraction ϕ_1 of the short diblock copolymer, while keeping other parameters (χN and f_1) fixed. Under the guide of SCFT results, we synthesized diblock copolymers to prepare the blending samples and experimentally achieved the DD structure with the volume fraction of the channels varying from 0.389 to 0.506. Our SCFT calculations demonstrate that the addition of the long A_2B diblock copolymer can readily enhance the stability of the DD structure over the DG structure by releasing the high packing frustration in the former. Furthermore, our work unveils that the formation of DD is sensitive to f_1, which needs to be located in the phase region of DG of the short A_1B diblock copolymer but not close to the C_6/DG boundary in order to suppress the formation of C_6. Our work demonstrates that the A_1B/A_2B blend with equal B-blocks but unequal A-blocks exhibits a superior capacity of stabilizing the DD structure evidenced by its considerable parameter space for stable DD. Considering that many nonclassical ordered structures have been stabilized by this A_1B/A_2B blend, more intriguing novel structures are likely to be experimentally discovered in this blending system by varying f_1, especially under the guide of SCFT.

ASSOCIATED CONTENT

Supporting Information

The Supporting Information is available free of charge at https://pubs.acs.org/doi/10.1021/acs.macromol.5c01972.

SEC chromatogram, ^{1}H NMR spectra, comparison of free energy among different phases in AB diblock copolymers, considered candidate ordered phases in SCFT, average mean curvature of different phases, comparison of free energy along changing ϕ_1 at a fixed γ value among different phases (PDF)

AUTHOR INFORMATION

Corresponding Authors

Xueyan Feng − *State Key Laboratory of Molecular Engineering of Polymers, Key Laboratory of Computational Physical Sciences, Department of Macromolecular Science, Fudan University, Shanghai 200438, China;* orcid.org/0000-0003-2348-8312; Email: fengxueyan@fudan.edu.cn

Guowei Wang − *State Key Laboratory of Molecular Engineering of Polymers, Key Laboratory of Computational Physical Sciences, Department of Macromolecular Science, Fudan University, Shanghai 200438, China;* orcid.org/0000-0003-2595-8269; Email: gwwang@fudan.edu.cn

Weihua Li − *State Key Laboratory of Molecular Engineering of Polymers, Key Laboratory of Computational Physical Sciences, Department of Macromolecular Science, Fudan University, Shanghai 200438, China;* orcid.org/0000-0002-5133-0267; Email: weihuali@fudan.edu.cn

Authors

Xinyu Wang − *State Key Laboratory of Molecular Engineering of Polymers, Key Laboratory of Computational Physical Sciences, Department of Macromolecular Science, Fudan University, Shanghai 200438, China*

Yi Feng − *State Key Laboratory of Molecular Engineering of Polymers, Key Laboratory of Computational Physical Sciences, Department of Macromolecular Science, Fudan University, Shanghai 200438, China*

Shuchen Lu − *State Key Laboratory of Molecular Engineering of Polymers, Key Laboratory of Computational Physical Sciences, Department of Macromolecular Science, Fudan University, Shanghai 200438, China*

Complete contact information is available at: https://pubs.acs.org/10.1021/acs.macromol.5c01972

Notes

The authors declare no competing financial interest.

https://doi.org/10.1021/acs.macromol.5c01972
Macromolecules 2025, 58, 9776−9785

■ ACKNOWLEDGMENTS

This work was supported by the Ministry of Science and Technology of China (2024YFA1209000) and the National Natural Science Foundation of China (22333002). The authors also acknowledge the staff of Beamline BL19U2 at the Shanghai Synchrotron Radiation Facility (SSRF) for their assistance with the SAXS experiments.

■ REFERENCES

(1) Huang, G.; Lai, H.; Song, J.; Jiang, Y.; Ji, S. A Universal Approach to Fabricating 3D Chemical Patterns for Directed Self-Assembly of Block Copolymers with Density Multiplication. *Macromolecules* **2023**, *56*, 5784−5791.
(2) Lin, E.-L.; Hsu, W.-L.; Chiang, Y.-W. Trapping structural coloration by a bioinspired gyroid microstructure in solid state. *ACS Nano* **2018**, *12*, 485−493.
(3) Park, W. I.; Yoon, J. M.; Park, M.; Lee, J.; Kim, S. K.; Jeong, J. W.; Kim, K.; Jeong, H. Y.; Jeon, S.; No, K. S.; Lee, J. Y.; Jung, Y. S. Self-assembly-induced formation of high-density silicon oxide memristor nanostructures on graphene and metal electrodes. *Nano Lett.* **2012**, *12*, 1235−1240.
(4) Lee, S.; Bluemle, M. J.; Bates, F. S. Discovery of a Frank-Kasper σ phase in sphere-forming block copolymer melts. *Science* **2010**, *330*, 349−353.
(5) Xie, N.; Li, W.; Qiu, F.; Shi, A.-C. σ phase formed in conformationally asymmetric AB-type block copolymers. *ACS Macro Lett.* **2014**, *3*, 906−910.
(6) Schulze, M. W.; Lewis, R. M., III; Lettow, J. H.; Hickey, R. J.; Gillard, T. M.; Hillmyer, M. A.; Bates, F. S. Conformational asymmetry and quasicrystal approximants in linear diblock copolymers. *Phys. Rev. Lett.* **2017**, *118*, 207801.
(7) Li, Q.; Chen, C.; Li, C.; Liu, R.; Bi, S.; Zhang, P.; Zhou, Y.; Mai, Y. Ordered bicontinuous mesoporous polymeric semiconductor photocatalyst. *ACS Nano* **2020**, *14*, 13652−13662.
(8) Wang, Y.; He, C.; Xing, W.; Li, F.; Tong, L.; Chen, Z.; Liao, X.; Steinhart, M. Nanoporous metal membranes with bicontinuous morphology from recyclable block-copolymer templates. *Adv. Mater.* **2010**, *22*, 2068−2072.
(9) Crossland, E. J.; Kamperman, M.; Nedelcu, M.; Ducati, C.; Wiesner, U.; Smilgies, D.-M.; Toombes, G. E.; Hillmyer, M. A.; Ludwigs, S.; Steiner, U.; et al. A Bicontinuous Double Gyroid Hybrid Solar Cell. *Nano Lett.* **2009**, *9*, 2807−2812.
(10) Hajduk, D. A.; Harper, P. E.; Gruner, S. M.; Honeker, C. C.; Kim, G.; Thomas, E. L.; Fetters, L. J. The gyroid: a new equilibrium morphology in weakly segregated diblock copolymers. *Macromolecules* **1994**, *27*, 4063−4075.
(11) Meuler, A. J.; Hillmyer, M. A.; Bates, F. S. Ordered network mesostructures in block polymer materials. *Macromolecules* **2009**, *42*, 7221−7250.
(12) Han, L.; Che, S. An overview of materials with triply periodic minimal surfaces and related geometry: from biological structures to self-assembled systems. *Adv. Mater.* **2018**, *30*, 1705708.
(13) Thomas, E. L.; Alward, D. B.; Kinning, D. J.; Martin, D. C.; Handlin Jr, D. L.; Fetters, L. J. Ordered bicontinuous double-diamond structure of star block copolymers: a new equilibrium microdomain morphology. *Macromolecules* **1986**, *19*, 2197−2202.
(14) Alward, D. B.; Kinning, D. J.; Thomas, E. L.; Fetters, L. J. Effect of arm number and arm molecular weight on the solid-state morphology of poly (styrene-isoprene) star block copolymers. *Macromolecules* **1986**, *19*, 215−224.
(15) Hasegawa, H.; Tanaka, H.; Yamasaki, K.; Hashimoto, T. Bicontinuous microdomain morphology of block copolymers. 1. Tetrapod-network structure of polystyrene-polyisoprene diblock polymers. *Macromolecules* **1987**, *20*, 1651−1662.
(16) Schulz, M. F.; Bates, F. S.; Almdal, K.; Mortensen, K. Epitaxial relationship for hexagonal-to-cubic phase transition in a book copolymer mixture. *Phys. Rev. Lett.* **1994**, *73*, 86.
(17) Matsen, M. W.; Schick, M. Stable and unstable phases of a linear multiblock copolymer melt. *Macromolecules* **1994**, *27*, 7157−7163.
(18) Floudas, G.; Pispas, S.; Hadjichristidis, N.; Pakula, T.; Erukhimovich, I. Microphase separation in star block copolymers of styrene and isoprene. Theory, experiment, and simulation. *Macromolecules* **1996**, *29*, 4142−4154.
(19) Hajduk, D. A.; Harper, P. E.; Gruner, S. M.; Honeker, C. C.; Thomas, E. L.; Fetters, L. J. A reevaluation of bicontinuous cubic phases in starblock copolymers. *Macromolecules* **1995**, *28*, 2570−2573.
(20) Matsen, M. W.; Bates, F. S. Block copolymer microstructures in the intermediate-segregation regime. *J. Chem. Phys.* **1997**, *106*, 2436−2448.
(21) Matsen, M. W. Phase behavior of block copolymer/homopolymer blends. *Macromolecules* **1995**, *28*, 5765−5773.
(22) Spontak, R. J.; Smith, S. D.; Ashraf, A. Dependence of the OBDD morphology on diblock copolymer molecular weight in copolymer/homopolymer blends. *Macromolecules* **1993**, *26*, 956−962.
(23) Lai, C. T.; Shi, A.-C. Binary blends of diblock copolymers: An effective route to novel bicontinuous phases. *Macromol. Theory Simul.* **2021**, *30*, 2100019.
(24) Hou, L.; Xu, Z.; Dong, Q.; Shi, A.-C.; Li, W. Stabilizing DG, DD, and DP Bicontinuous Network Phases in Pure AB-Type Block Copolymers beyond Relieving Packing Frustration. *Macromolecules* **2024**, *57*, 2165−2175.
(25) Chu, C.-Y.; Pei, R.-Y.; Chen, H.-L. Order−Order Transition from Ordered Bicontinuous Double Diamond to Hexagonally Packed Cylinders in Stereoregular Diblock Copolymer/Homopolymer Blends. *Macromolecules* **2018**, *51*, 8493−8500.
(26) Lin, C.-H.; Higuchi, T.; Chen, H.-L.; Tsai, J.-C.; Jinnai, H.; Hashimoto, T. Stabilizing the ordered bicontinuous double diamond structure of diblock copolymer by configurational regularity. *Macromolecules* **2018**, *51*, 4049−4058.
(27) Lee, H.; Kwon, S.; Min, J.; Jin, S.-M.; Hwang, J. H.; Lee, E.; Lee, W. B.; Park, M. J. Thermodynamically stable plumber's nightmare structures in block copolymers. *Science* **2024**, *383*, 70−76.
(28) Takagi, H.; Yamamoto, K. Effect of block copolymer composition and homopolymer molecular weight on ordered bicontinuous double-diamond structures in binary blends of polystyrene−polyisoprene block copolymer and polyisoprene homopolymer. *Macromolecules* **2021**, *54*, 5136−5143.
(29) Lindsay, A. P.; Cheong, G. K.; Peterson, A. J.; Weigand, S.; Dorfman, K. D.; Lodge, T. P.; Bates, F. S. Complex phase behavior in particle-forming AB/AB′ diblock copolymer blends with variable core block lengths. *Macromolecules* **2021**, *54*, 7088−7101.
(30) Takagi, W.; Suzuki, J.; Aoyama, Y.; Mihira, T.; Takano, A.; Matsushita, Y. Bicontinuous double-diamond structures formed in ternary blends of AB diblock copolymers with block chains of different lengths. *Macromolecules* **2019**, *52*, 6633−6640.
(31) Takagi, H.; Yamamoto, K. Phase boundary of Frank−Kasper σ phase in phase diagrams of binary mixtures of block copolymers and homopolymers. *Macromolecules* **2019**, *52*, 2007−2014.
(32) Lindsay, A. P.; Lewis III, R. M.; Lee, B.; Peterson, A. J.; Lodge, T. P.; Bates, F. S. A15, σ, and a quasicrystal: Access to complex particle packings via bidisperse diblock copolymer blends. *ACS Macro Lett.* **2020**, *9*, 197−203.
(33) Mueller, A. J.; Lindsay, A. P.; Jayaraman, A.; Lodge, T. P.; Mahanthappa, M. K.; Bates, F. S. Emergence of a C15 Laves phase in diblock polymer/homopolymer blends. *ACS Macro Lett.* **2020**, *9*, 576−582.
(34) Xie, J.; Shi, A.-C. Phase behavior of binary blends of diblock copolymers: Progress and opportunities. *Langmuir* **2023**, *39*, 11491−11509.
(35) Yamaguchi, D.; Hashimoto, T. A phase diagram for the binary blends of nearly symmetric diblock copolymers. 1. Parameter space of molecular weight ratio and blend composition. *Macromolecules* **2001**, *34*, 6495−6505.

https://doi.org/10.1021/acs.macromol.5c01972
Macromolecules 2025, 58, 9776−9785

(36) Wu, Z.; Li, B.; Jin, Q.; Ding, D.; Shi, A.-C. Microphase and macrophase separations in binary blends of diblock copolymers. *Macromolecules* **2011**, *44*, 1680−1694.
(37) You, X.; Xu, Z.; Dong, Q.; Li, W. Largely Asymmetric Binary Mesocrystals beyond Inorganic Crystals Formed in Linear ABC/ABC Blends. *Macromolecules* **2024**, *57*, 6681−6692.
(38) Xie, N.; Liu, M.; Deng, H.; Li, W.; Qiu, F.; Shi, A.-C. Macromolecular metallurgy of binary mesocrystals via designed multiblock terpolymers. *J. Am. Chem. Soc.* **2014**, *136*, 2974−2977.
(39) Xie, Q.; Qiang, Y.; Li, W. Regulate the stability of gyroids of ABC-type multiblock copolymers by controlling the packing frustration. *ACS Macro Lett.* **2020**, *9*, 278−283.
(40) Liu, M.; Qiang, Y.; Li, W.; Qiu, F.; Shi, A.-C. Stabilizing the Frank-Kasper phases via binary blends of AB diblock copolymers. *ACS Macro Lett.* **2016**, *5*, 1167−1171.
(41) Zhao, F.; Dong, Q.; Li, Q.; Liu, M.; Li, W. Emergence and stability of exotic "binary" HCP-type spherical phase in binary AB/AB blends. *Macromolecules* **2022**, *55*, 10005−10013.
(42) Zhang, Z.; Li, L.; Song, Q.; Peng, L.; Huang, X.; Li, W. Directed Self-Assembly of Binary AB/AB Diblock Copolymer Blends for Dense Nanopatterns with Density Multiplication. *Macromolecules* **2024**, *57*, 4878−4888.
(43) Fredrickson, G. *The Equilibrium Theory of Inhomogeneous Polymers*; Oxford University Press, 2006.
(44) Matsen, M. Immiscibility of large and small symmetric diblock copolymers. *J. Chem. Phys.* **1995**, *103*, 3268−3271.
(45) Park, S. J.; Bates, F. S.; Dorfman, K. D. Alternating gyroid in block polymer blends. *ACS Macro Lett.* **2022**, *11*, 643−650.
(46) Park, S. J.; Bates, F. S.; Dorfman, K. D. Complex phase behavior in binary blends of AB diblock copolymer and ABC triblock terpolymer. *Macromolecules* **2023**, *56*, 1278−1288.
(47) Matsen, M. W. Stabilizing new morphologies by blending homopolymer with block copolymer. *Phys. Rev. Lett.* **1995**, *74*, 4225.
(48) Rasmussen, K. Ø.; Kalosakas, G. Improved numerical algorithm for exploring block copolymer mesophases. *J. Polym. Sci., Part B: Polym. Phys.* **2002**, *40*, 1777−1783.
(49) Tzeremes, G.; Rasmussen, K. Ø.; Lookman, T.; Saxena, A. Efficient computation of the structural phase behavior of block copolymers. *Phys. Rev. E: Stat., Nonlinear, Soft Matter Phys.* **2002**, *65*, 041806.
(50) Thompson, R. B.; Rasmussen, K. O.; Lookman, T. Improved convergence in block copolymer self-consistent field theory by Anderson mixing. *J. Chem. Phys.* **2004**, *120*, 31−34.
(51) Zhang, J.; Zhou, P.; Shi, B.; Li, P.; Wang, G. High-Efficient Access to Inverse Morphologies via Living Anionic Polymerization-Mediated Polymerization-Induced Cooperative Assembly. *Macromolecules* **2023**, *56*, 5743−5753.


CAS BIOFINDER DISCOVERY PLATFORM™
BRIDGE BIOLOGY AND CHEMISTRY FOR FASTER ANSWERS
Analyze target relationships, compound effects, and disease pathways
Explore the platform
CAS
A division of the American Chemical Society

https://doi.org/10.1021/acs.macromol.5c01972
Macromolecules 2025, 58, 9776−9785